Space Weather

RESEARCH ARTICLE
10.1029/2022SW003266

Investigating Potential Causes for the Prediction of Spurious Magnetopause Crossings at Geosynchronous Orbit in MHD Simulations

Pauline M. Dredger[1], Ramon E. Lopez[1], Yaireska M. Collado-Vega[2,3], Shreeya Khurana[4], and Lutz M. Rastaetter[2]

[1]University of Texas at Arlington, Arlington, TX, USA, [2]NASA Goddard Space Flight Center, Greenbelt, MD, USA, [3]Space Weather Laboratory, Greenbelt, MD, USA, [4]Carnegie Mellon University, Pittsburgh, PA, USA

This article is a companion to Collado-Vega et al. (2023), https://doi.org/10.1029/2022SW003212.

Key Points:

- MHD models driven by OMNI solar wind can wrongly predict magnetopause motion if solar wind observed at L1 does not reach the magnetosphere
- The models predict magnetopause motion better if the driver of the motion is solar wind density than when the driver is a negative interplanetary magnetic field Bz
- Coupling the MHD codes to a ring current model for storm-time events results in significantly better predictions of magnetopause location

Correspondence to:
P. M. Dredger,
pauline.dredger@mavs.uta.edu

Citation:
Dredger, P. M., Lopez, R. E., Collado-Vega, Y. M., Khurana, S., & Rastaetter, L. M. (2023). Investigating potential causes for the prediction of spurious magnetopause crossings at geosynchronous orbit in MHD simulations. *Space Weather*, *21*, e2022SW003266. https://doi.org/10.1029/2022SW003266

Received 22 AUG 2022
Accepted 14 FEB 2023

Abstract

During intense geomagnetic storms, the magnetopause can move in as far as geosynchronous orbit, leaving the satellites in that orbit out in the magnetosheath. Spacecraft operators turn to numerical models to predict the response of the magnetopause to solar wind conditions, but the predictions of the models are not always accurate. This study investigates four storms with a magnetopause crossing by at least one GOES satellite, using four magnetohydrodynamic models at NASA's Community Coordinated Modeling Center to simulate the events, and analyzes the results to investigate the reasons for errors in the predictions. Two main reasons can explain most of the erroneous predictions. First, the solar wind input to the simulations often contains features measured near the L1 point that did not eventually arrive at Earth; incorrect predictions during such periods are due to the solar wind input rather than to the models themselves. Second, while the models do well when the primary driver of magnetopause motion is a variation in the solar wind density, they tend to overpredict or underpredict the integrated Birkeland currents and their effects during times of strong negative interplanetary magnetic field (IMF) B_z, leading to poorer prediction capability. Coupling the MHD codes to a ring current model, when such a coupling is available, generally will improve the predictions but will not always entirely correct them. More work is needed to fully characterize the response of each code under strong southward IMF conditions as it relates to prediction of magnetopause location.

Plain Language Summary

The magnetopause is the boundary that separates the region dominated by Earth's magnetic field from the solar wind. Plasma and magnetic field conditions are very different on either side of the magnetopause, which can cause problems for satellites when the boundary moves and they find themselves in a different region of space than expected. Numerical models of the magnetosphere are used to predict the motion of the magnetopause, which moves based on the driving of the solar wind, but such predictions do not always correspond to real-life observations. This study compares predictions from four different models to observations from spacecraft that crossed the magnetopause during a handful of events with intense solar wind conditions, to determine the reasons that simulation results could be incorrect. The first source of error is the uncertainty in solar wind input to the models. The second source of error is a difference in the response of the codes to different solar wind parameters. Coupling the magnetosphere models to models that add the physics of specific magnetosphere regions can help to improve the accuracy of the overall predictions of magnetopause motion.

1. Introduction

The magnetopause, the boundary between the magnetosphere and the shocked solar wind in the magnetosheath, separates two regions of very different plasma and magnetic field conditions. In general, the magnetosheath is turbulent, with dense plasma and magnetic field that vary with the arrival of the solar wind, while inside the magnetosphere Earth's magnetic field dominates and plasma densities are much lower. The balance of plasma pressure from the magnetosheath and magnetic pressure from the terrestrial magnetic field determines, in the most basic approximation, the instantaneous location of the magnetopause, which varies with the two pressures (Martyn, 1951). High solar wind dynamic pressure in the magnetosheath will force the boundary inward toward Earth from the outside. On the other hand, a strong southward interplanetary magnetic field (IMF) components will increase the Region 1 field-aligned currents and the nightside cross-tail current, creating fringe fields opposite to Earth's magnetic field and thus weakening it, which reduces the outward magnetic pressure from the inside

and allows the magnetopause to move closer to Earth (Maltsev & Lyatsky, 1975; Maltsev et al., 1996; Sibeck et al., 1991; Wiltberger et al., 2003). A numerical model of the magnetosphere must reproduce these phenomena if it is to accurately predict magnetopause position.

The ring current, which is strongest during a geomagnetic storm, can also affect the position of the magnetopause. As ions are injected from the tail into the Inner Magnetosphere (IM), they join the ring current and drift clockwise around Earth (as seen from the north); because of the direction of the drift, more energetic particles are lost to the dawn sector magnetopause than to the dusk sector, and the ring current becomes asymmetrical. The resulting partial ring current closes along magnetic field lines as the Region 2 field-aligned current, flowing into the polar cap on the dusk side and out on the dawn side. The stronger thermal pressure from the ions in the partial ring current in the dusk sector causes the magnetopause to be farther away from Earth than it is in the dawn sector (Dmitriev et al., 2011).

During times of quiet solar wind, the magnetopause is several Earth radii away from geosynchronous orbit, where many commercial and scientific satellites are located, and so these spacecraft remain inside the magnetosphere. On the other hand, when the solar wind driver of a geomagnetic storm arrives at Earth, the location of the boundary is much more variable (Bonde et al., 2018). Operators of satellites orbiting near Earth rely on predictions of the magnetopause location to let them know if their spacecraft might cross the boundary, particularly if the spacecraft use magnetic torquing for attitude adjustments (Sibeck, 1995). Often to make these predictions, satellite operators use the magnetohydrodynamic (MHD) models available at the CCMC: the Lyon-Fedder-Mobarry simulation (LFM), the Space Weather Modeling Framework (SWMF), the Open Geospace General Circulation Model (OpenGGCM), and the Grand Unified Magnetosphere-Ionosphere Circulation Model (GUMICS). While empirical models of magnetopause position exist, physics-based models can provide a better (if imperfect) prediction capability during extreme magnetic storms (Lopez et al., 2007). Collado-Vega et al. (2023) conducted a study examining the performance of these four models in predicting magnetopause location for eight storms; specifically, the study looked for correctly simulated magnetopause encounters at the locations of GOES 13 and 15, both at geosynchronous orbit. They found that SWMF and GUMICS tended to underpredict magnetopause motion in response to strong solar wind conditions, while LFM and OpenGGCM predicted both correct and spurious magnetopause crossings.

In order to better understand the models' predictive capabilities, including under what conditions their use is appropriate, this study investigates possible causes for their incorrect predictions. In particular, we examine the overpredictions of LFM and OpenGGCM by considering the four events in the Collado-Vega paper in which the GOES spacecraft actually crossed the magnetopause. Where Collado-Vega et al. (2023) focuses on performance metrics of the MHD codes' predictive abilities, our analysis takes rather a qualitative than a quantitative approach, addressing underlying reasons for the MHD predictions on a model-by-model basis.

2. Methodology

This study primarily uses the geocentric solar ecliptic (GSE) coordinate system. In GSE coordinates, X points along the Earth-sun line and Z is perpendicular to the ecliptic plane, where positive Z points northward. Y completes the right-handed coordinate system, with positive Y in the duskward direction.

To determine the time at which a satellite crosses the magnetopause, the following method was used. Earth's magnetic field points northward, so a magnetometer will always read a positive B_z while inside the magnetopause. If the incoming IMF has a negative Z-component, the compressed B_z in the sheath will be negative. Consequently, in magnetometer data, B_z will rotate from positive (negative) to negative (positive) as the spacecraft crosses the boundary into the magnetosheath (magnetosphere). The spacecraft encounters the magnetopause at the moment the magnetometer reads $B_z = 0$ nT. All the events in this study had strong southward IMF components, so magnetopause crossings in the relevant data were identified in this way, following Lopez et al. (2007).

For this study, four events were chosen in which solar wind conditions pushed the magnetopause so far toward Earth that it reached geosynchronous orbit and crossed over one or both of GOES 13 and 15. GOES 13 and 15 are part of NOAA's Geostationary Operational Environmental Satellite program and fly in geosynchronous orbits (Redmon et al., 2017). During the events of this study, GOES 13 was located at 75° West and GOES 15 was located at 135° West, which means that GOES 13 was always four hours ahead of GOES 15 in local time.

Each event was simulated using all four magnetospheric models at the CCMC, without a ring current and using the default auroral conductance in order to compare the models as fairly as possible, since the couplings available vary among the codes. After these initial runs, the simulations for certain events were repeated with the MHD codes coupled to a ring current model where such a coupling was available at the CCMC. The four models used in this study are the LFM model, the SWMF, OpenGGCM, and GUMICS. These are briefly described here with their various possible couplings, as available at the CCMC. The resolution of the models was in all cases the lowest available, which varies among the four models.

LFM solves the semi-conservative MHD equations on a stretched spherical grid and uses its Magnetosphere-Ionosphere Coupler/Solver (MIX) to model the ionosphere (Lyon et al., 2004). MIX takes the field-aligned currents calculated at the inner boundary of the MHD code and maps them down to the ionosphere grid, which extends in each hemisphere to 45° latitude, using the currents with a given conductance to calculate the potential (Merkin & Lyon, 2010). LFM can also be two-way coupled with the Rice Convection Model (RCM), a bounce average drift kinetic model of the IM that adds ring current physics (Toffoletto et al., 2003; Wolf et al., 1982). LFM provides the magnetic field and plasma boundary conditions to RCM, which calculates the pressure and density of the ring current and returns these values to the MHD code. MIX passes its potential solution to both LFM and RCM (Pembroke et al., 2012). The version of LFM-MIX coupled to RCM is available for use at the CCMC. The resolution of the runs in this study is $53 \times 48 \times 64$ cells and the size of the cells at the GOES orbit, on the dayside, is about 0.4 R_E in each direction.

SWMF includes a number of modules that simulate various parts of the space weather system (Tóth et al., 2005, 2012). The magnetosphere part of the framework (SWMF Global Magnetosphere or GM module) uses the Block-Adaptive-Tree-Solarwind-Roe-Upwind-Scheme (BATS-R-US), which solves the conservative MHD equations on a block-adaptive grid (Powell et al., 1999). Rice Convection Model is coupled into the framework as the IM module and functions similarly to the way it is coupled to LFM, as described above. The IM component receives the magnetic field and plasma initial and boundary values from BATS-R-US and passes back corrected pressure values for the IM to the GM module (Zeeuw et al., 2004). The SWMF Ionosphere Electrodynamics (IE) module uses the field-aligned currents from BATS-R-US to calculate the ionospheric potential and conductance, returning the potential to the GM and IM modules (Ridley et al., 2001, 2004; Ridley & Liemohn, 2002). The ionosphere grid is a complete sphere around Earth, but the auroral conductance model providing the conductance for the potential calculation only reaches 60° magnetic latitude (Mukhopadhyay et al., 2020). SWMF request runs at the CCMC couple BATS-R-US with the two-dimensional IE potential solver and can include RCM. Runs in this study use the version of the code implemented on the website in 2014 and a one million cell overview grid. The size of the cells at the GOES locations for the events here presented is 0.25 R_E in each direction.

OpenGGCM solves the semi-conservative MHD equations on a stretched Cartesian grid and maps the field-aligned currents onto a sphere within the inner boundary to a convection potential solver. OpenGGCM can also be coupled to RCM, but this coupling was not used in this work (Cramer et al., 2017; Raeder et al., 2001, 2008). The simulations in this study were run on a seven million cell overview grid, with cell sizes at the GOES locations of about 0.15 R_E in the X direction and 0.25 R_E in Y and Z.

GUMICS-4, the version of GUMICS used here, couples an MHD model of the magnetosphere to an ionosphere model. The magnetosphere part of the code solves the conservative MHD equations on a refined hierarchically adaptive octogrid with a locally varying time-step, while the simulation of the ionosphere is based on solving the height-integrated current continuity equation on a spherical surface with a prescribed grid point density highest in the auroral oval (Janhunen et al., 2012). GUMICS does not have the option for a ring current model coupling at the CCMC. GUMICS was run on a grid of 100,000 cells; the cell size at the GOES locations was 0.5 R_E along each axis.

3. Results

3.1. Solar Wind Discrepancies

A closer examination of the individual events reveals that the solar wind input to the models may have caused some of the incorrect predictions. Because of the inhomogeneous nature of the solar wind, the conditions observed by a monitor at the first Lagrange point may differ significantly from the solar wind that actually impacts the magnetosphere. Comparisons between the OMNI data set, which is composed of L1 observations from ACE and

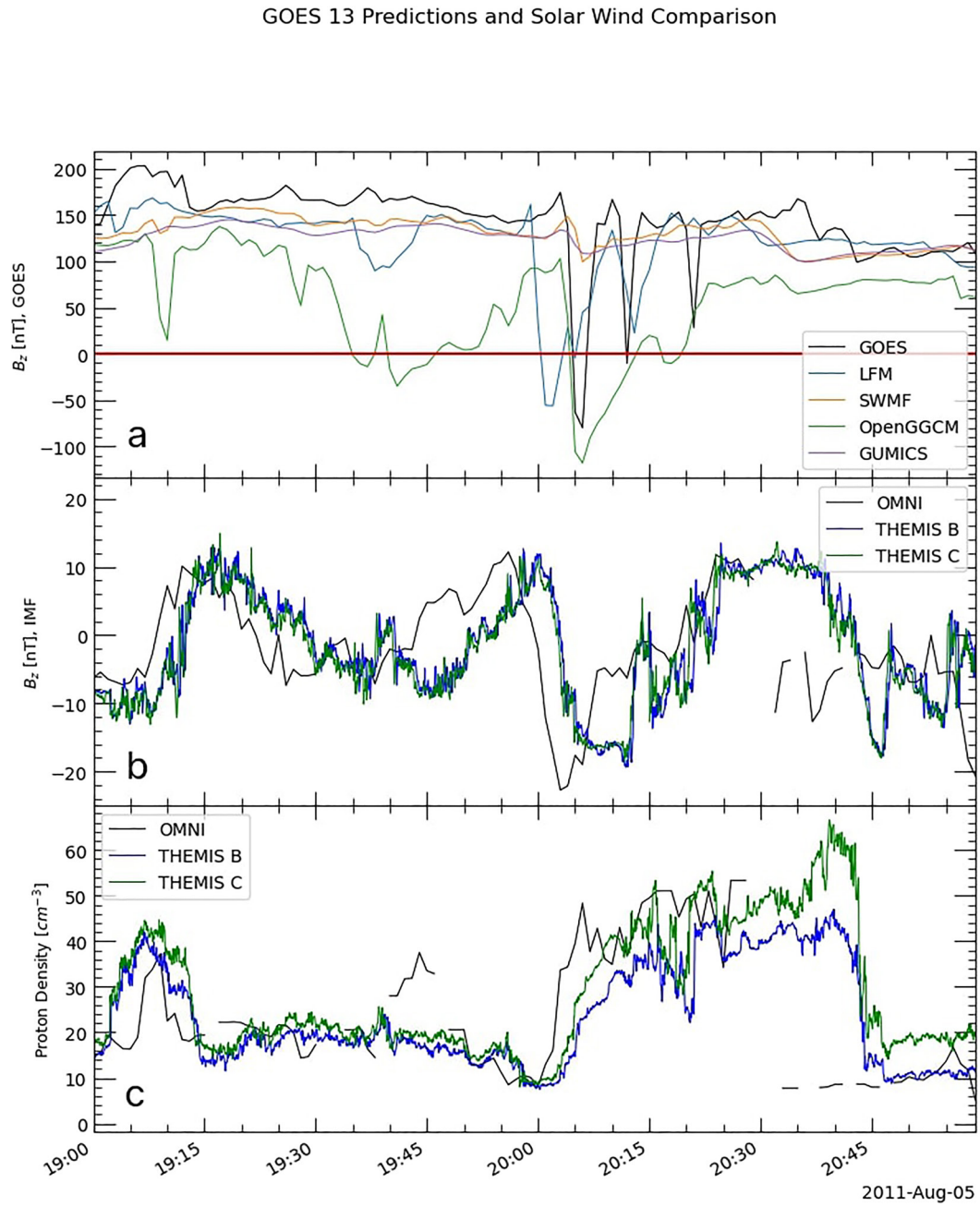

Figure 1. From top to bottom: (a) Observations of B_z from GOES 13 with predictions from LFM, Space Weather Modeling Framework, OpenGGCM, and GUMICS. The red horizontal line is included in this and any following GOES plots for ease of identifying magnetopause crossings, which occur at $B_z = 0$ nT under southward interplanetary magnetic field (IMF) conditions. (b) IMF B_z from OMNI compared with measurements from THEMIS B and C. Note that the propagation of OMNI data to a nominal bow shock does not necessarily correspond with the location of THEMIS B/C and so a shift in the time series is present. (c) Proton densities from OMNI and from THEMIS B/C.

Wind propagated to a nominal bow shock position, and data from other spacecraft that were temporarily in the solar wind during the various events, reveal significant discrepancies between the datasets that explain several of the false positives in the model predictions. Although the L1 observations may not be inherently flawed, such data are not always appropriate for simulating downstream conditions.

The first event, 2011 August 5, contains a feature in the solar wind input that may have caused one of the models to predict a spurious magnetopause crossing by both GOES 13 and GOES 15. We see in Figure 1 the actual

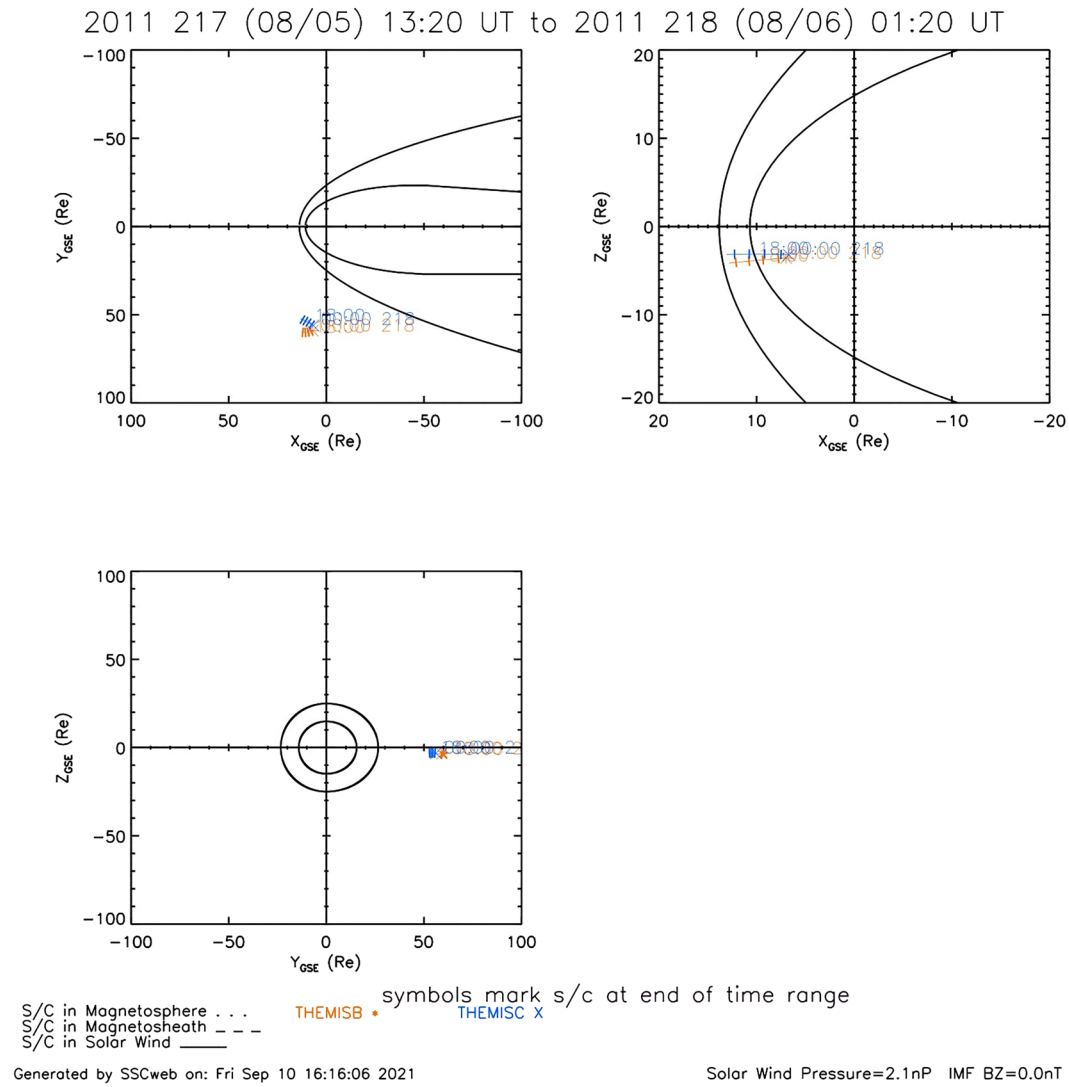

Figure 2. Locations of THEMIS B and C during the 2011 August 5 event. Although the two spacecraft are more than 50 R_E off the Earth-sun line, they are the only other source of solar wind observations for this event (plot from SSCWeb).

GOES observations and the model predictions plotted together. B_z from the model is plotted in GSE coordinates and the real data are in the cylindrical coordinate system used by GOES—the quantity plotted here is H_p, which is generally equivalent to B_z. Around 19:40 UT, B_z as predicted by OpenGGCM dips below 0 nT, indicating a magnetopause crossing by the satellite under consideration. LFM predicts an approach to the magnetopause around the same time but not a crossing. SWMF and GUMICS do not predict a change in B_z at this time. The solar wind from the OMNI data set, which was provided by Wind during this event, shows a density pulse from about 20 cm^{-3}–40 cm^{-3} that caused the simulated magnetopause to move inward over the locations of GOES 13 and 15. This density pulse, observed at L1, does not seem to have actually reached Earth. THEMIS B and C were in the solar wind at the time as shown in Figure 2, although they were between 50 and 60 R_E away from the Earth-Sun line. They did not record the increase in the solar wind density that Wind saw further upstream. The magnetometer and THEMIS observations, combined with the lack of a real magnetopause crossing at geosynchronous orbit, strongly suggest that the density pulse in the OMNI data at 19:40 UT did not impact the magnetopause. Thus, the erroneous predictions of magnetopause crossings were not necessarily due to issues with OpenGGCM but more likely the consequence of the wrong solar wind input.

A second event, 2011 September 26, tells a similar story. OpenGGCM predicts a magnetopause crossing at the location of GOES 13 shortly after 14:00 UT, in response to a southward turning of IMF B_z accompanied by

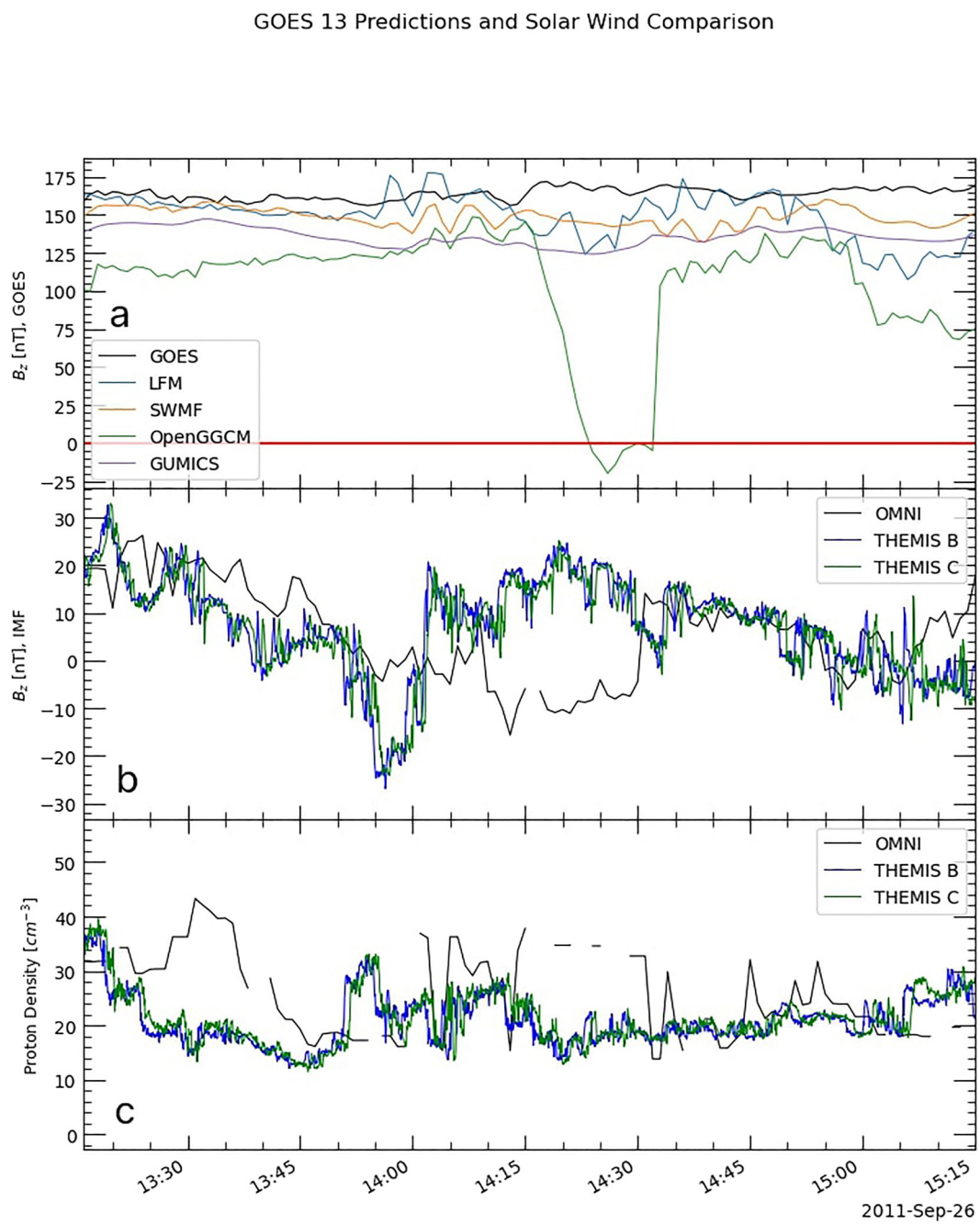

Figure 3. (a) GOES 13 observations and corresponding MHD predictions of B_z, along with (b) interplanetary magnetic field B_z and (c) solar wind proton densities from OMNI and THEMIS B/C for 2011 September 26. Even taking into account potential timing issues with the OMNI propagation, there are still significant differences in the OMNI and THEMIS sets of solar wind observations.

high proton densities in the OMNI data, which was once again provided by Wind (Figure 3). LFM, SWMF, and GUMICS do not predict a magnetopause approach during the period shown in Figure 3. This time, THEMIS B and C were well-positioned (Figure 4) to provide solar wind observations 170 R_E closer to Earth than Wind, less than 20 R_E from the Earth-Sun line. B_z in the OMNI was southward, reaching around −10 nT between 14:10 and 14:30 UT, while the IMF B_z observed by THEMIS B and C was positive, with an overall difference of at least 20 nT between THEMIS and OMNI. Proton densities at THEMIS B and C were also much less than those in OMNI by roughly 15 cm^{-3} during the same period. This difference would have resulted in a simulated magnetopause located closer to Earth than in reality. The source of the solar wind input seems once again to

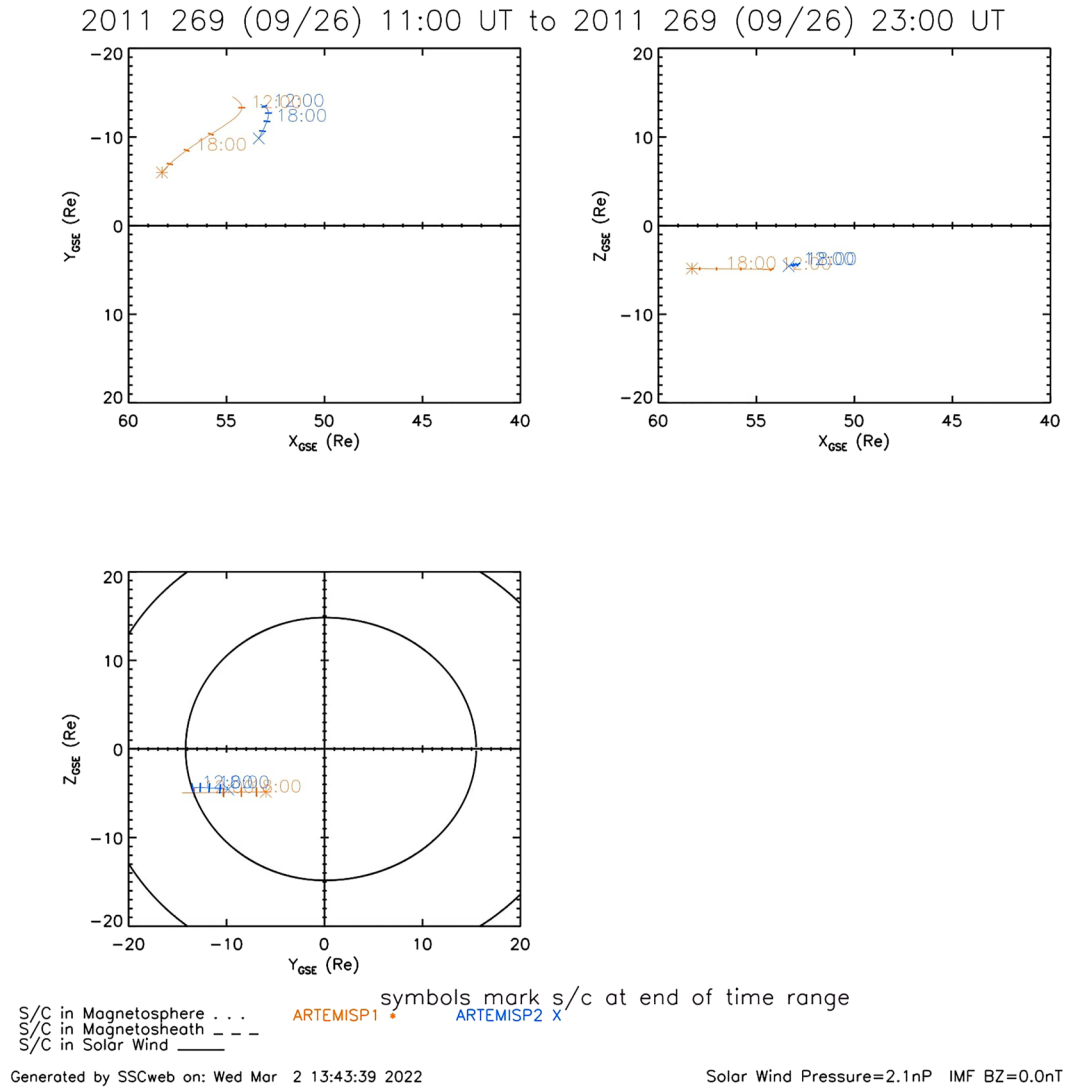

Figure 4. Locations of THEMIS B/C during the 2011 September 26 event. During this period, the two spacecraft were relatively close to the Earth-sun line and so their observations should be a good representation of the solar wind that impacted the bow shock (plot from SSCWeb).

explain the spurious crossing after 14:00 UT, although it is clearly not the only issue with the simulation results, given the other false crossings predicted later in the day by LFM and OpenGGCM (see discussion in Section 3.2).

In addition to predicting false crossings, the models can also miss real crossings because of problems with the solar wind input. GOES 15 crossed the magnetopause right after 23:00 UT on 2017 September 7, but none of the models reproduced that crossing (Figure 5). THEMIS A, D, and E were intermittently in the solar wind between 23:00 and 23:30 UT, all within 2 R_E of the nose of the bow shock (Figure 6), and observed a negative IMF B_z of −20 nT or stronger right after 23:00 UT, while the IMF B_z from OMNI (provided by Wind) was −10 nT or weaker. Thus, even the two models that predicted the crossings minutes later, that is, LFM and OpenGGCM, did not capture the initial crossing, probably due at least in part to this discrepancy between the two sets of solar wind observations. Unfortunately, the THEMIS spacecraft were not in the solar wind for very long and cannot be used to confirm the OMNI data later in the event.

3.2. Solar Wind Driver of Magnetopause Motion: IMF B_z Versus Density

Classification of the types of solar wind driver for the magnetopause crossings in each event leads to a further explanation of the false alarms and misses in the simulation results. The models seem to make good predictions

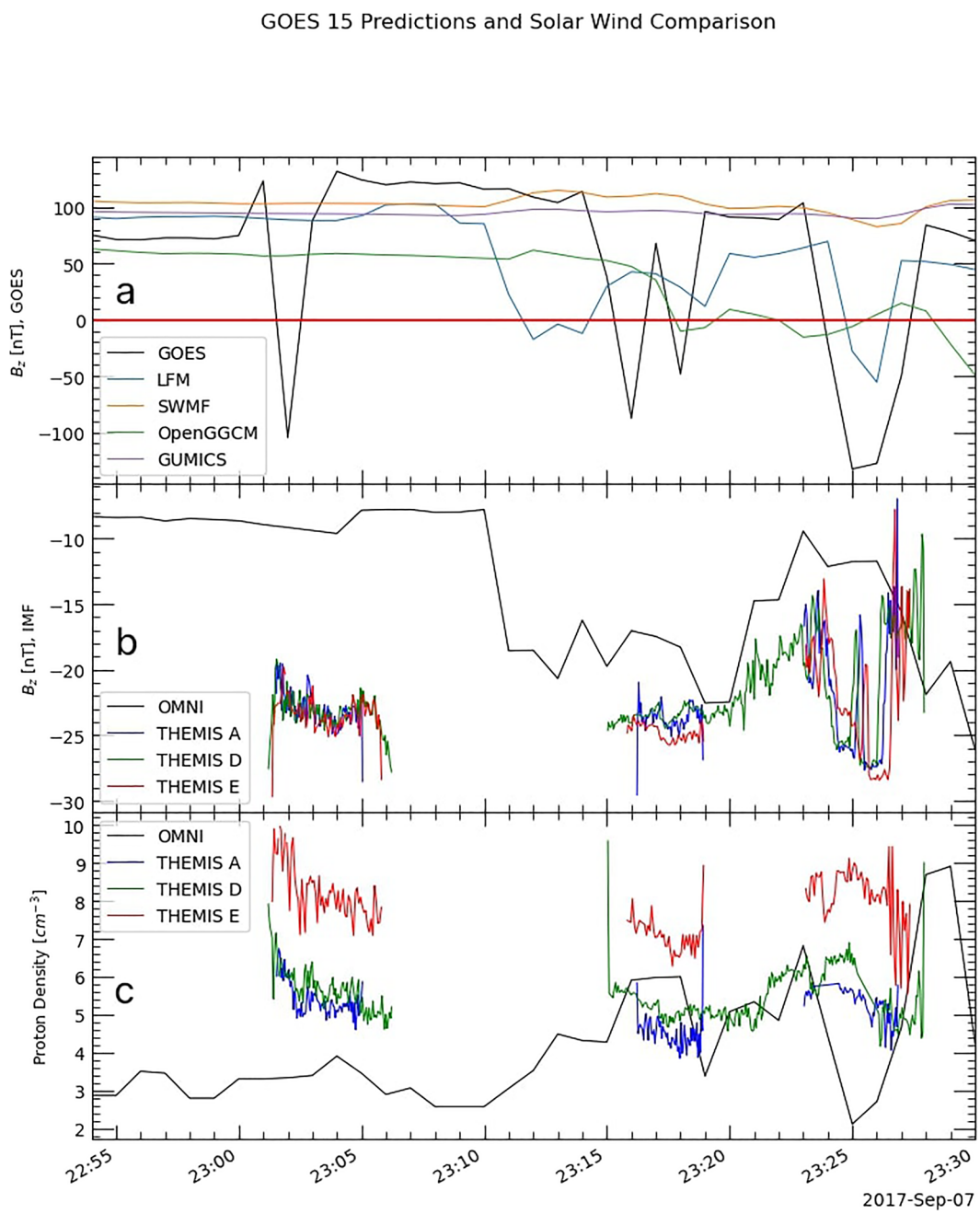

Figure 5. (a) GOES 15 observations and model predictions of B_z with (b) interplanetary magnetic field B_z and (c) solar wind proton densities from OMNI and THEMIS A/D/E. THEMIS data are only plotted for the brief periods during which the spacecraft were in the solar wind. During this period the solar wind velocity (not shown here) changed drastically, so, as in previously discussed cases, there may be timing issues from the OMNI propagation.

when a sudden density increase drives the magnetopause inward, but perform poorly for events in which the magnetopause is eroded by the presence of a negative IMF B_z component. The predictions for 2011 September 26, shown in Figure 7, follow this pattern. After the initial false crossing in OpenGGCM due to use of the incorrect solar wind input right after 14:00 UT, both OpenGGCM and LFM predict a series of crossings before and after the real crossing at 16:40 UT. The false crossings between 15:40 and 17:00 UT could be due to the fact that the OMNI densities were higher than those observed by THEMIS B/C from 15:10 to roughly 16:00 UT, in a similar manner to the examples in Section 3.1, although there is also a period of southward IMF B_z at this time. On the other hand, during the times of the spurious crossings between 18:00 and 19:00 UT, the solar wind proton

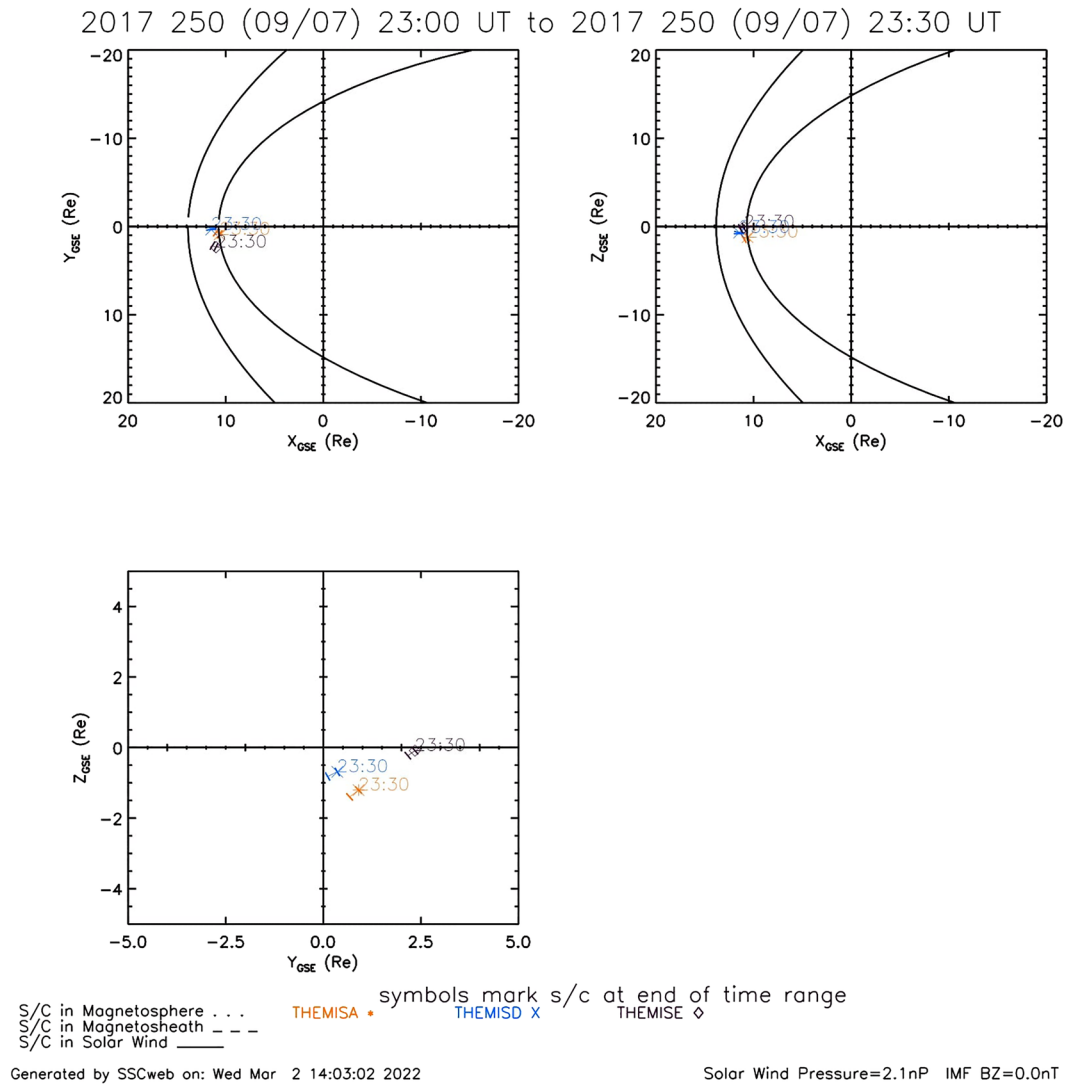

Figure 6. THEMIS A/D/E locations from 23:00 UT to 23:30 UT on 2017 September 7 (plot from SSCWeb).

densities in both OMNI and THEMIS B and C are much lower than they were earlier in the event without much variation, while IMF B_z is strongly negative. Both models predict that the GOES satellites reenter the magnetosphere after the real crossings starting at 19:20 UT, a series of brief encounters with the boundary that were probably caused by the density increase in the solar wind at that time. The false crossings in LFM and OpenGGCM between 18:00 and 19:00 UT seem to be caused by the strong negative IMF B_z, since there is little change in the solar wind densities during this period.

The total integrated field-aligned currents from each model on 2011 September 26 are plotted in Figure 8 alongside the integrated currents from AMPERE. The two models that do not predict either real or spurious crossings, SWMF and GUMICS, have less current flowing into and out of the ionosphere than LFM or OpenGGCM, which have currents either similar to or greater than the AMPERE integrated FACs. This event occurred near equinox, so the currents in both hemispheres are of similar strength. At 16:40 UT, the time of the real GOES 13 crossing, the AMPERE currents increase but the currents from LFM and SWMF actually decrease, probably in response to the northward turning of OMNI IMF B_z at this time, and GOES 13 in the LFM predictions exits the magnetosheath early. The modeled currents from LFM and SWMF increase later right before 18:00 UT, when LFM and OpenGGCM predict more false crossings. OpenGGCM currents remain higher than and show little qualitative similarity to the AMPERE integrated currents throughout the whole event. From about 16:10 to 19:30 UT, OMNI and THEMIS B and C all agree reasonably well, so the false crossings between 18:00 and 19:00 UT

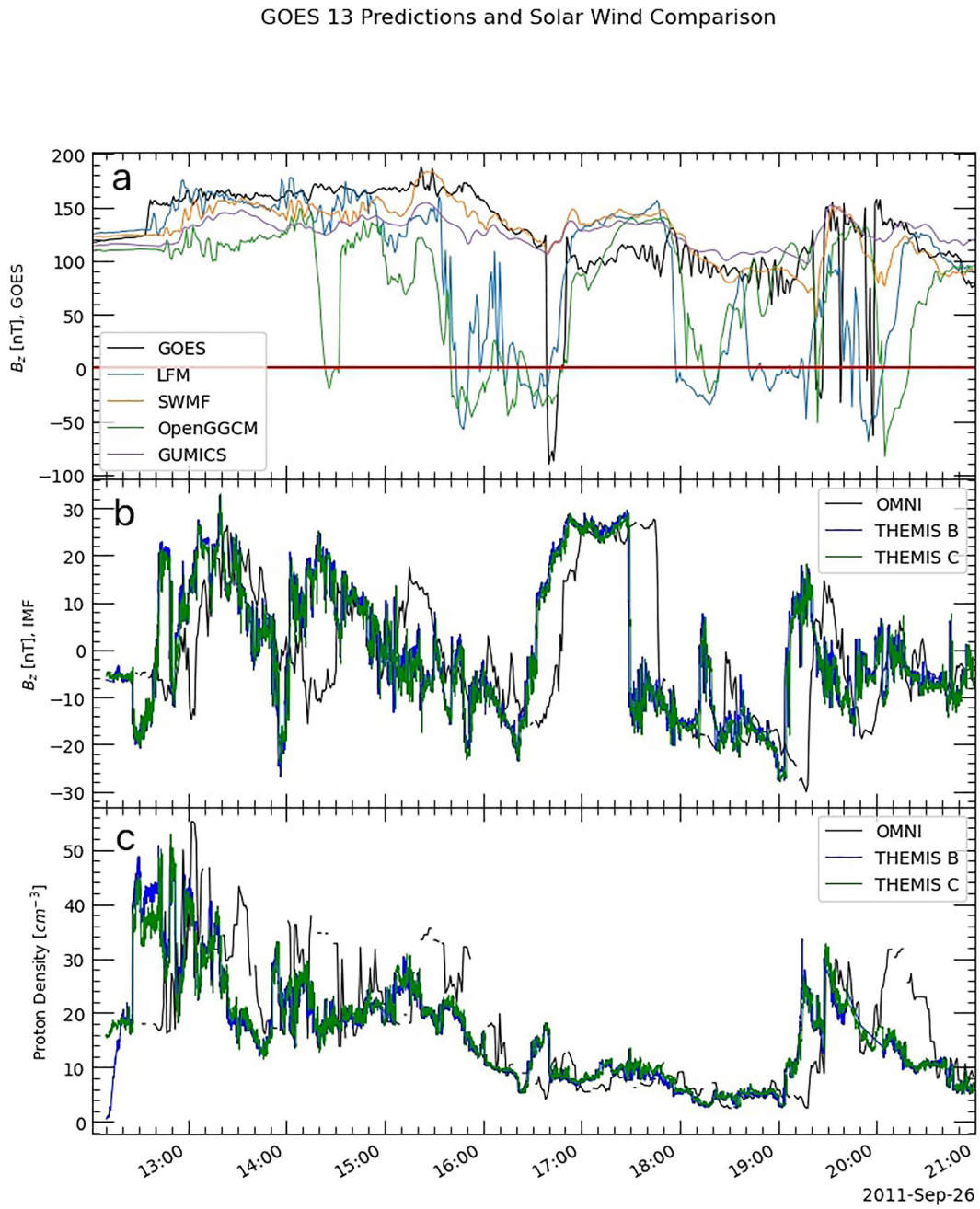

Figure 7. (a) GOES 13 observations and model predictions of B_z with (b) interplanetary magnetic field (IMF) B_z and (c) solar wind proton densities from OMNI and THEMIS B/C. LFM and OpenGGCM predict spurious magnetopause crossing during times when magnetopause motion is primarily driven by southward IMF B_z.

cannot be explained by discrepancies in the solar wind input to the simulations. The patterns of real and modeled currents correspond well to the real and modeled GOES observations, but the models respond more to the IMF variations while the observations respond to changes in solar wind proton density.

The simulations of the geomagnetic storm of 2015 June 22 follow the same tendencies. All four models capture the magnetopause crossings by GOES 13 and 15 that lasted from right after 18:30 until about 20:00 UT. These crossing were driven by a sharp increase in the solar wind density from 10 cm^{-3}–60 cm^{-3} at 18:30 UT, accompanied by a southward turning of IMF B_z, which went from 0 nT to more than −15 nT, pushing the magnetopause all the way to geosynchronous orbit and beyond. Sustained high densities and increasingly stronger IMF B_z values

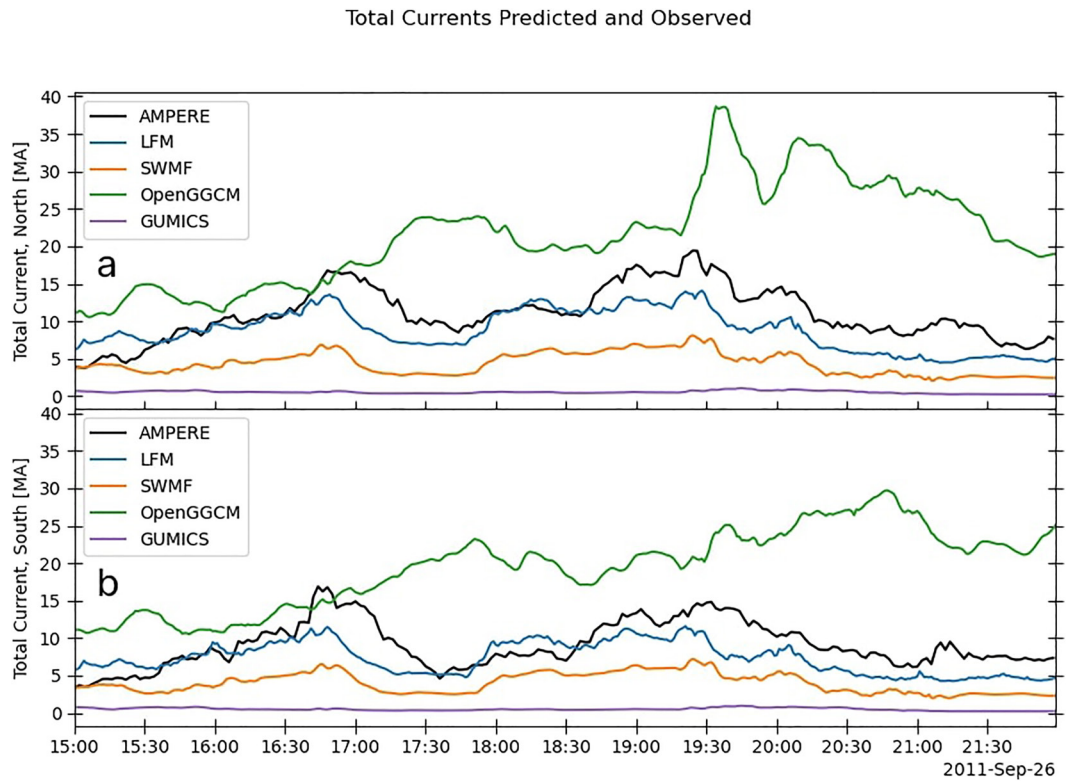

Figure 8. Total integrated field-aligned currents in the (a) northern and (b) southern hemispheres from AMPERE and as predicted by the MHD models for 2011 September 26.

that reached almost −40 nT kept GOES 13 and 15 in the magnetosheath until around 19:40 UT, when a northward turning of the IMF and a decrease in density to about 40 cm^{-3} allowed the magnetopause to move back outward again. This magnetopause motion is predicted reasonably well by the models, although the extent of the motion varies among the four simulations, as demonstrated by the differences in the timing of the predicted crossings. LFM and OpenGGCM perform the best during this part of the event, with SWMF close behind. However, around 21:00 UT, LFM and OpenGGCM predict a false crossing by GOES 13 (see Figure 9) in response to another change in IMF B_z at 20:50 UT, this time from 10 nT to −10 nT. There was a small jump in proton density that accompanied the 20:50 UT southward turning, but this variation was not significant compared to previous density increases and decreases. The integrated Birkeland currents for the event are shown in Figure 10. At 20:50 UT, the time of the reversal of IMF B_z, the currents in LFM and SWMF increase, with those in OpenGGCM increasing a few minutes later around 21:10 UT, while the AMPERE currents are decreasing, especially in the northern hemisphere. The currents in the models are responding more strongly to IMF B_z than the real currents did in this event.

All the predicted crossings not due to incorrect solar wind input in the other two events, 2011 August 5 and 2017 September 7, can be explained in the same manner. Magnetopause motion driven primarily by increases of solar wind density tends to be modeled reasonably well, while strong southward IMF B_z values cause the models, in particular LFM and OpenGGCM, to overpredict the inward motion of the boundary. Moreover, the simulated integrated Birkeland currents during the false crossings do not match the integrated currents seen in the AMPERE data set.

3.3. Adding a Ring Current Model

Running LFM and SWMF coupled to the RCM adds the effect of ring current physics, which is particularly important during geomagnetic storms. For 2011 September 26, including the ring current greatly improves the LFM predictions and, to a lesser extent, those of SWMF, apart from the false crossings caused by discrepancies in the solar wind densities between 15:40 and 17:00 UT mentioned in Section 3.2. The total current flowing into and out of the ionosphere is shown in Figure 11, which compares the AMPERE integrated FACs with those

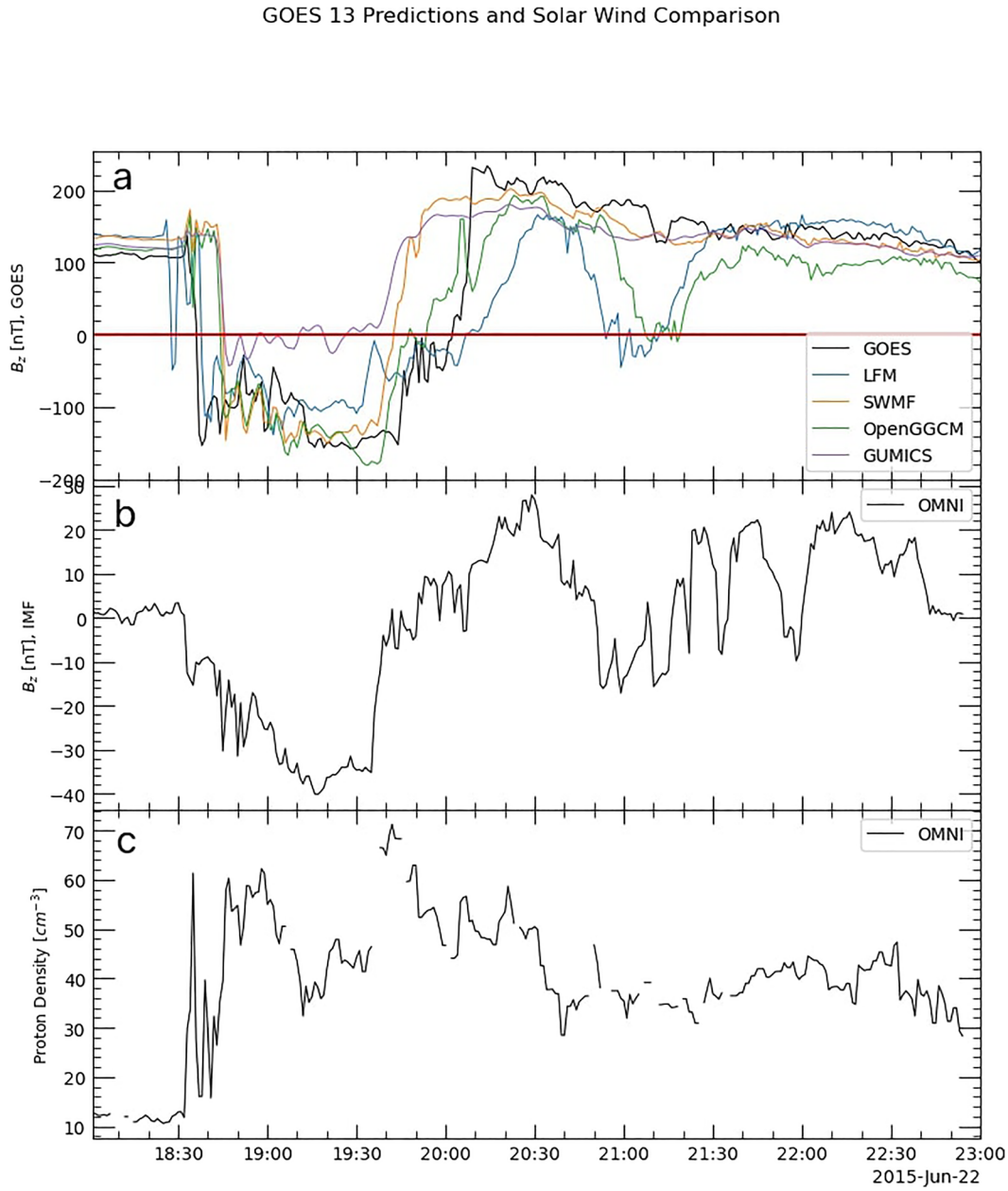

Figure 9. (a) GOES 13 predictions and observations of B_z, with (b) OMNI interplanetary magnetic field B_z and (c) proton densities on 2015 June 22.

predicted by LFM and SWMF, both with and without the ring current. The LFM run that included the ring current predicts the currents much better than the original run; as a result, the predictions of magnetopause crossings at the GOES locations are more accurate throughout the period shown in Figure 11. The ring current coupling helps SWMF as well, but throughout the event the predicted integrated field-aligned currents are much weaker than the real currents, especially in the northern hemisphere, and the model does not predict any magnetopause crossings.

The storm on 2011 August 5 responds similarly to the addition of the ring current. The LFM predictions improve at both of the two GOES locations and for the integrated Birkeland currents, although the simulation still under-predicts the periods of strongest current, that is, between 20:00 and 20:45 UT. SWMF with the ring current predicts one of the GOES 15 crossings at 20:10 UT, which before it had missed, but the SWMF values for the integrated Birkeland currents, while stronger with RCM than without, are still in general significantly lower than the AMPERE values, especially in the northern hemisphere (see Figure 12). The effect of including ring current

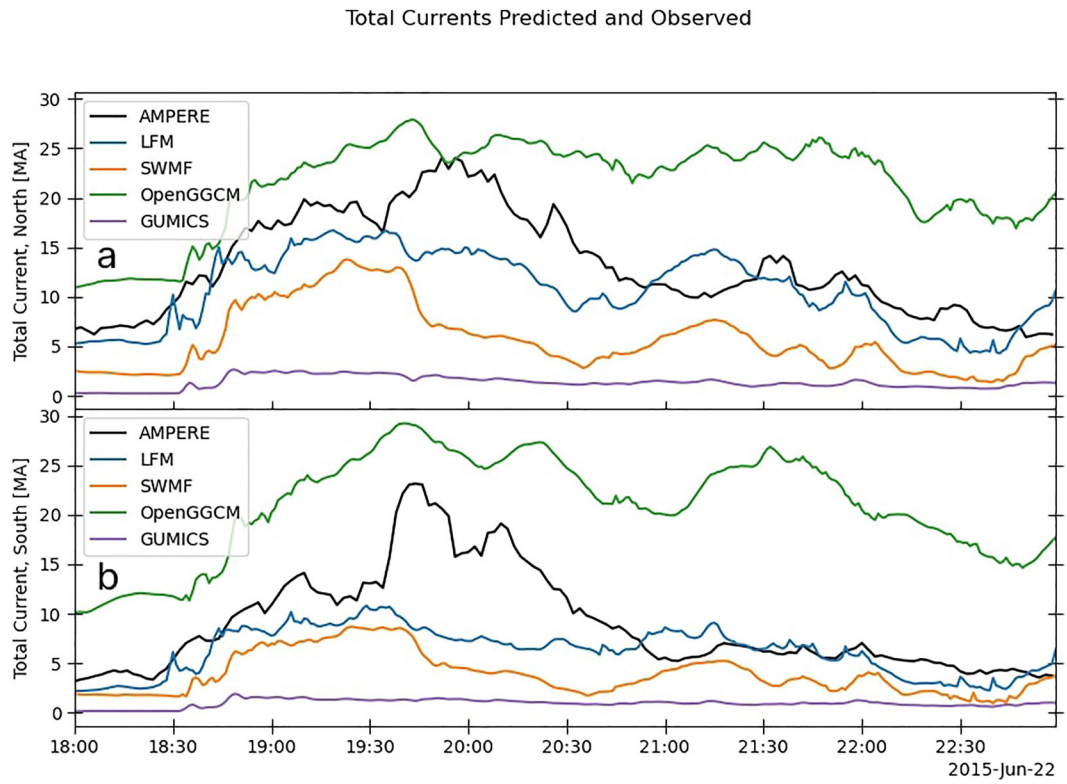

Figure 10. Total integrated field-aligned currents in the (a) northern and (b) southern hemispheres from AMPERE and as predicted by the MHD models for 2015 June 22.

physics is not as pronounced during this event for either LFM or SWMF as it is during the 2011 September event; this is, however, expected because the period of interest for the August event is early in the storm, before any significant decrease in SYM-H and, hence, before a strong ring current had time to form in real life. The crossings during the 2017 September 7 storm also take place before the real SYM-H becomes strongly negative, so RCM has little effect on the predictions at the location of GOES 15 between 23:00 and 23:30 UT. The later spurious crossing in LFM, right before 00:30 and further into the storm than the real crossings, is removed, but SWMF still misses the real crossings altogether (Figure 13).

The results of the LFM-RCM and SWMF-RCM runs for the 2015 June 22 storm do not display the expected effect of the ring current. With some small improvements, the predictions at the GOES locations are largely similar to those from the runs without the ring current. The integrated Birkeland current magnitudes are somewhat improved, but the models still miss the peak in the southern hemisphere current around 20:00 UT. Additionally, adding RCM does not remove the increase in the currents of both hemispheres predicted shortly after 21:00 UT and corresponding with spurious GOES crossings in LFM, although it does, barely, remove the crossing in GOES 13, as shown in Figure 14.

4. Discussion

The inhomogeneous nature of the solar wind (Borovsky, 2008) means that plasma features and IMF observed near L1 do not necessarily reach the magnetosphere. Even for events without multiple solar wind observations, discrepancies can sometimes be confirmed by means of fortuitously placed ground magnetometers. The first event discussed in Section 3.1 is an example of such a situation. The H, Z, and F components of the Honolulu magnetometer, which was near local noon during the period of interest, responded to the density increases at 19:00 and at 20:00 UT with increases of their own, but record only a very small reaction to the 19:40 density pulse seen in the OMNI data (Figure 15), supporting the conclusion that the pulse either did not reach Earth or was much smaller than the one observed at L1. This is a well-known issue (Merkin et al., 2013), yet space weather forecasts must for the time being rely on point observations at L1 to characterize the solar wind. Since

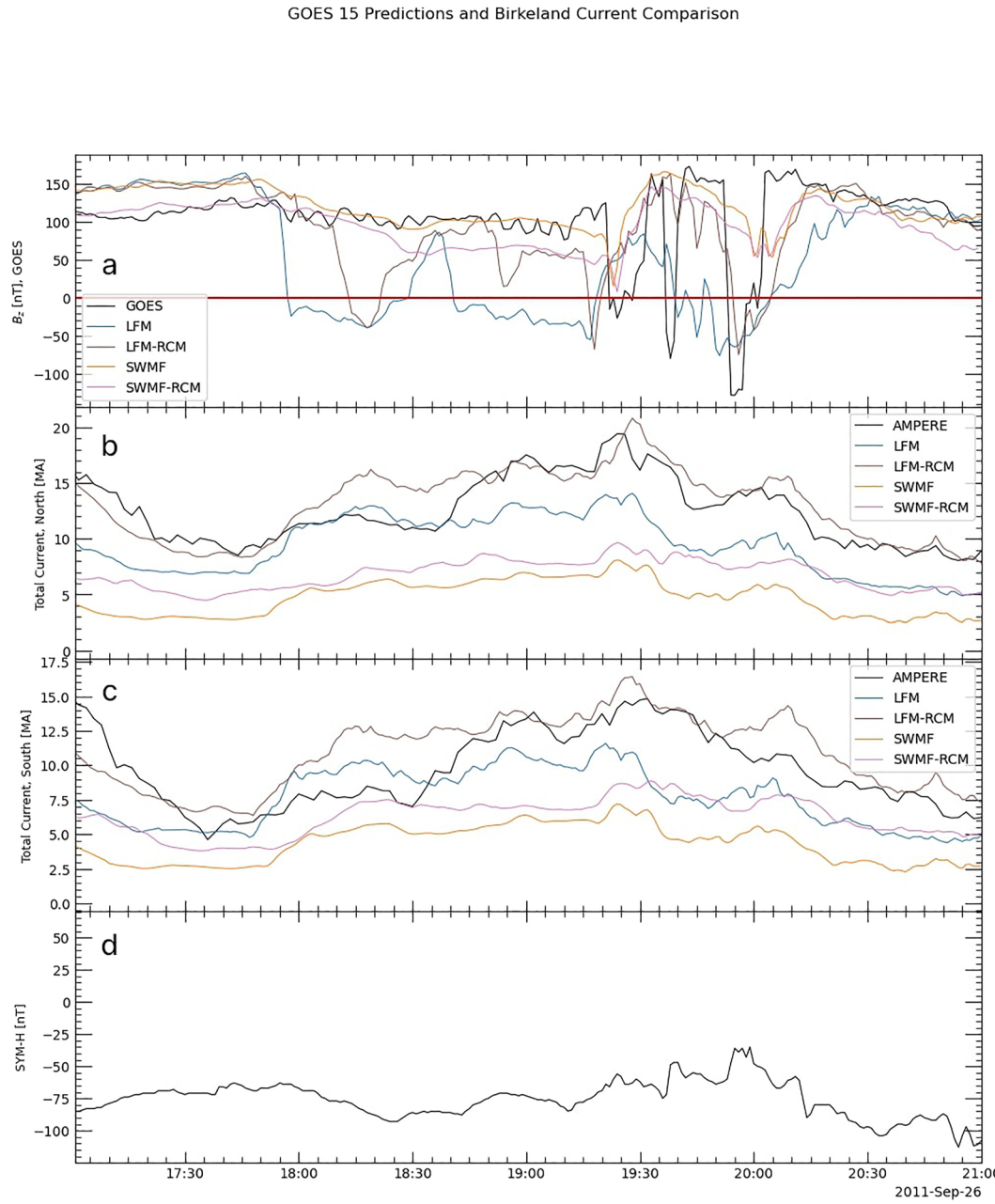

Figure 11. From top to bottom: (a) GOES 15 observations and the corresponding predictions of B_z from LFM and Space Weather Modeling Framework, with and without RCM; (b) total integrated FACs into the northern hemisphere from AMPERE and the models; (c) total integrated FACs into the southern hemisphere from AMPERE and the models; (d) real SYM-H during the 2011 September 26 event.

discrepancies large enough to significantly change predictions of magnetopause position exist in three out of four of the events here considered, it would be useful to have a quantitative idea of the probability that the solar wind in the OMNI data set does not represent the solar wind that impacts the bow shock. A possible approach to such a study would compare OMNI data to observations from spacecraft like THEMIS B/C or Geotail, during periods when they are near the Earth-Sun line, to calculate the correlation of the two datasets.

Inaccuracies in the prediction of the integrated field-aligned currents reduce the models' reliability when the magnetopause moves because of erosion of Earth's magnetic field. The investigations of the response of the MHD codes to southward turnings in the IMF have here been restricted to the consideration of the effect of the ring

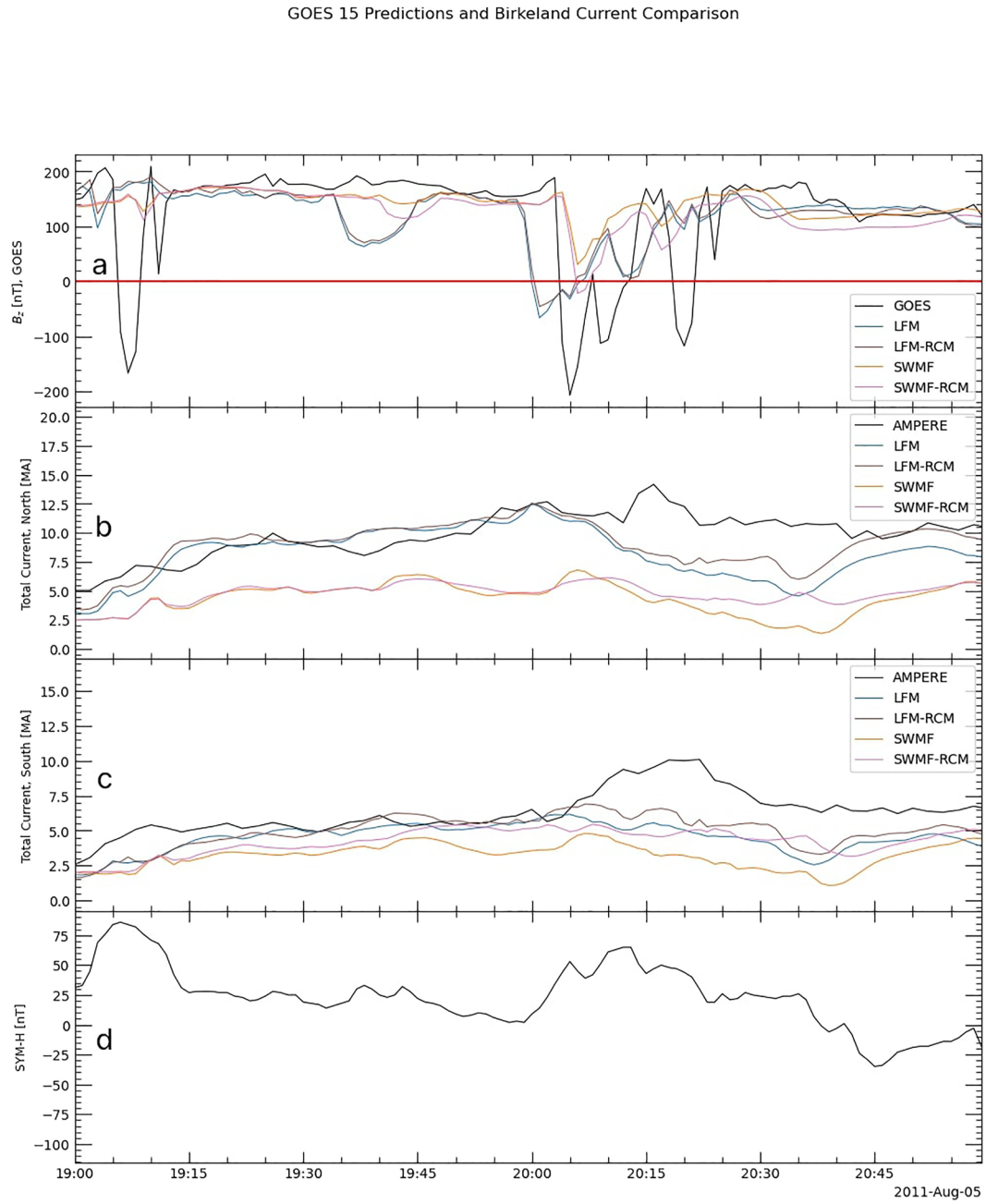

Figure 12. Same as Figure 11, but for 2011 August 5. The real ring current had not yet become strong during the time of the magnetopause crossings.

current on the integrated Birkeland current predictions, but the nature of the modeled ionosphere must play a role as well. Further studies should consider the results of coupling more sophisticated ionosphere models to LFM and OpenGGCM or even of setting a range of constant Pedersen conductances for repeated simulation runs.

Including ring current physics tends to improve storm-time predictions of magnetopause location, especially when the movements of the magnetopause is caused by erosion of Earth's magnetic field due to a strong southward IMF component, but coupling RCM to the MHD codes does not completely solve the problem. On the one hand, a significant IMF B_y component can cause interhemispheric asymmetries in the ionosphere which may not necessarily be reproduced in the models, since MHD models coupled to RCM only couple the northern hemisphere to the ring current (Pembroke et al., 2012; Zeeuw et al., 2004). Introducing IMF B_y changes the location

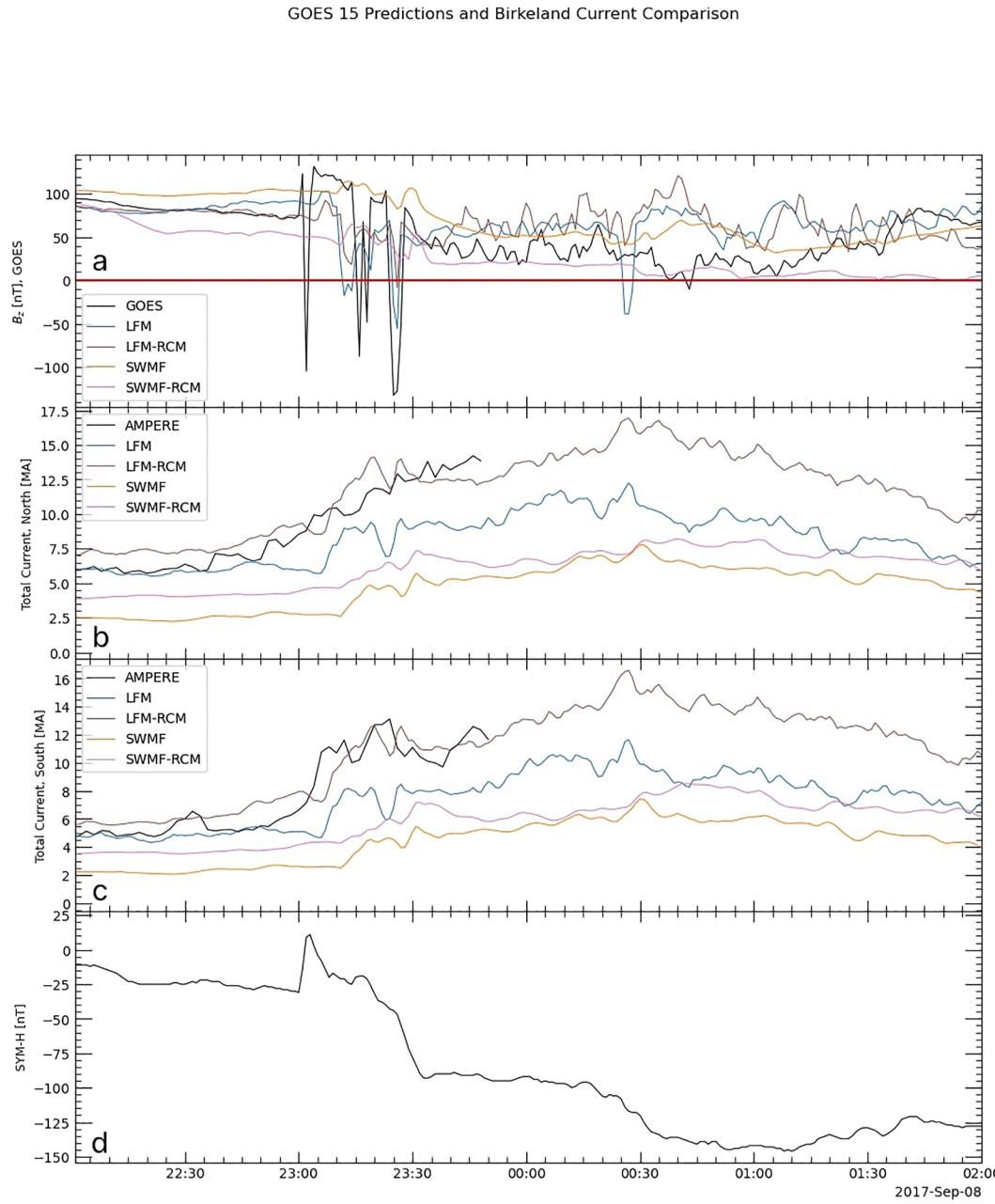

Figure 13. Same as Figure 11, but for 2017 September 7–8. AMPERE data (panels b and c) are not available for 2017 September 8. The real ring current had not yet become strong during the time of the magnetopause crossings.

of the ring current, moving it away from the equatorial plane either north or south, depending on the sign of B_y. If the models are not capturing all the B_y effects, the simulated ring current may not be in the correct location. Such an inaccuracy could particularly affect predictions in the +Y sector, where the asymmetric inflation of the ring current can influence the location of the magnetopause.

During the storm of 2015 June 22, after 19:35 UT, the IMF had a very strong positive B_y component for several hours, during which time LFM predicted false magnetopause crossings by both GOES 13 and 15 (Figure 16). Adding the ring current to the LFM predictions removes the actual 21:00 UT crossing at GOES 13, but the simulated satellite still approaches the boundary too closely. At this time, GOES 13 was well into the afternoon sector, so the ring current should have had a greater influence on magnetopause location in the region through which the spacecraft was passing. It seems possible that the large IMF B_y at the time was causing effects in the

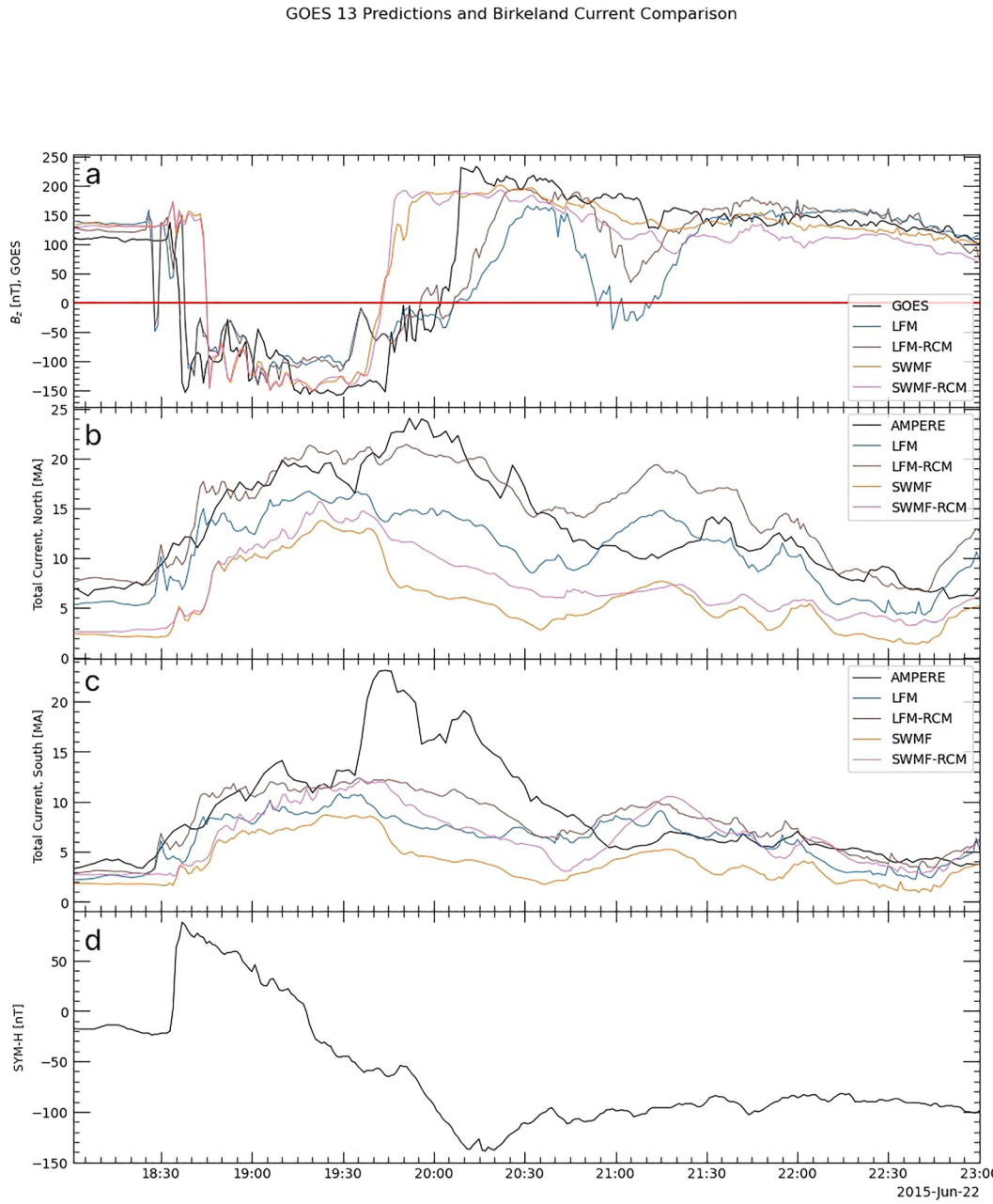

Figure 14. Same as Figure 11, but for GOES 13 on 2015 June 22. Although during the beginning of the real crossing the ring current is weak, as indicated by the positive SYM-H (panel d), it is strong by 19:30 UT.

real magnetosphere that were not reproduced in the simulation, perhaps resulting in a modeled ring current distribution that had some significant differences with reality.

5. Conclusions

In this study, four events during which the magnetopause moved in past geosynchronous orbit were selected and modeled with four different MHD codes. GOES 13 and 15 data were compared with simulation results at the GOES positions to analyze the ability of the models to predict magnetopause motion. There are two main causes of mistakes in the predictions. First, the exact solar wind observed near the first Lagrange point does not always reach the magnetosphere, so using it as input for magnetosphere simulations can lead to false predictions

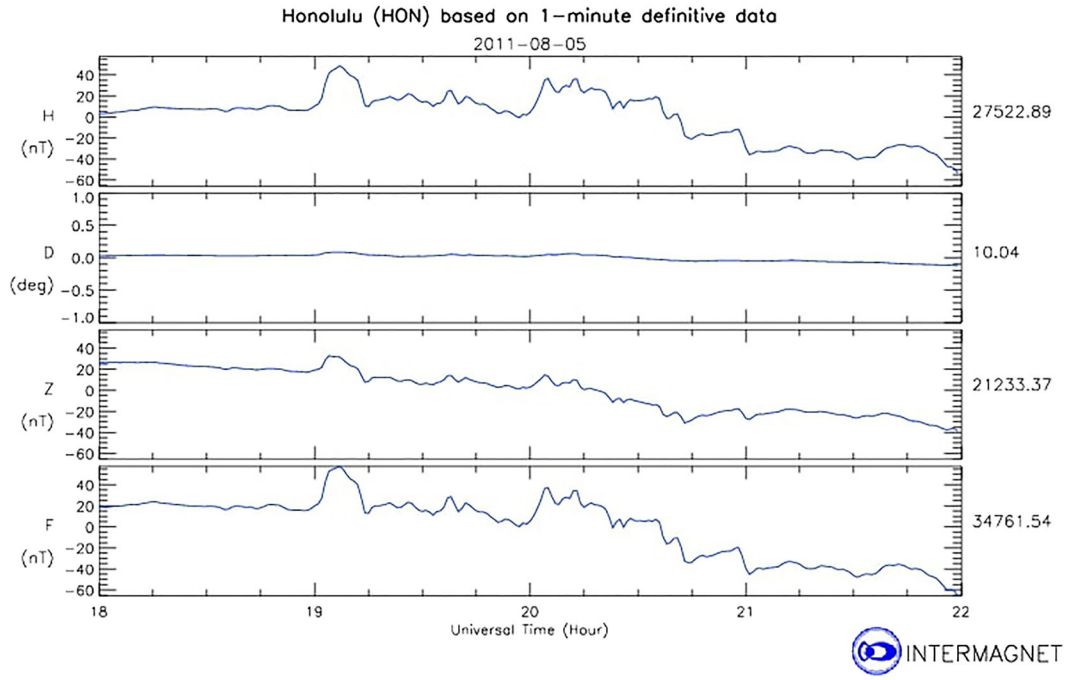

Figure 15. Magnetometer data from the Honolulu station. There is no real response to the 19:40 UT density pulse seen in OMNI, which suggests that the pulse did not reach Earth (plot from Intermagnet).

of magnetopause motion. Second, although the models accurately predict the response of the magnetopause to changes in solar wind density, they sometimes struggle to calculate the Birkeland currents; this can lead to incorrect predictions of the erosion of Earth's magnetic field and the consequent motion of the magnetopause. The chances of correctly predicting magnetopause location during a storm are significantly improved by using a ring current model.

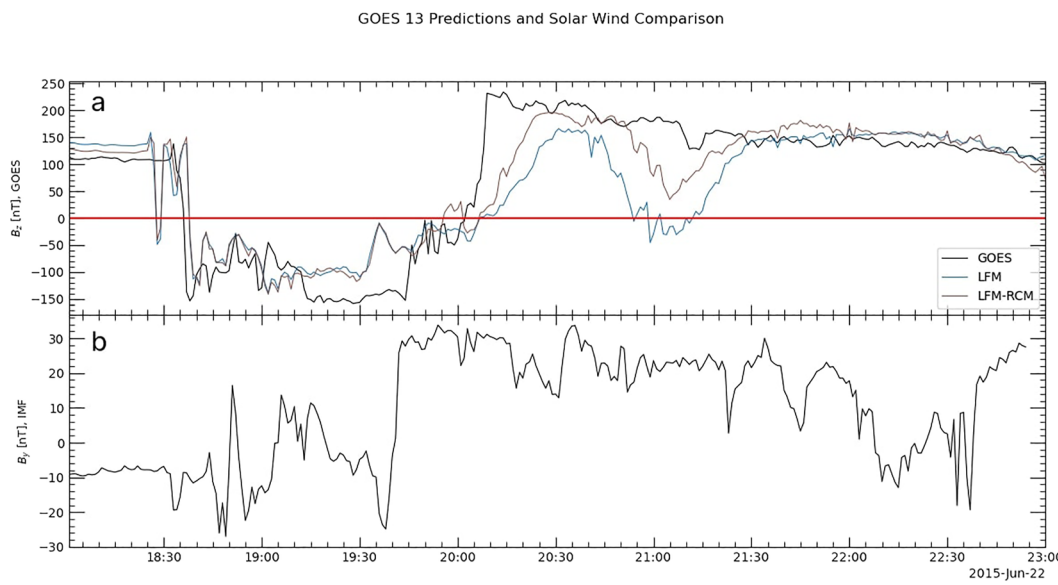

Figure 16. (a) GOES 13 observations of B_z and the corresponding predictions by LFM and LFM-RCM, on 2015 June 22, with (b) OMNI interplanetary magnetic field (IMF) B_y. During the time of the spurious crossing predicted by LFM, the IMF had a very strong, positive B_y component.

Data Availability Statement

GOES data were provided by NOAA (https://www.ngdc.noaa.gov/stp/satellite/goes/dataaccess.html). OMNI and THEMIS data were provided by CDAWeb (NASA CDAWeb Development Team, 2019). Orbit plots were provided by SSCWeb (https://sscweb.gsfc.nasa.gov/cgi-bin/Locator_graphics.cgi). We thank the AMPERE team and the AMPERE Science Data Center for providing data products derived from the Iridium Communications constellation, enabled by support from the National Science Foundation (http://ampere.jhuapl.edu/).

Acknowledgments
We acknowledge the support of the US National Science Foundation (NSF) under Grant 1916604. We also acknowledge the support of the National Aeronautics and Space Administration (NASA) under Grants 80NSSC19K1670 and 80NSSC20K0606 (The Center for the Unified Study of Interhemispheric Asymmetries (CUSIA)). Simulation results have been provided by the Community Coordinated Modeling Center at Goddard Space Flight Center through their public Runs on Request system (http://ccmc.gsfc.nasa.gov). The LFM Model was developed by John Lyon et al. at Dartmouth College/NCAR-HAO/JHU-APL/CISM. OpenGGCM was developed by Joachim Raeder and Timothy Fuller-Rowell at the Space Science Center, University of New Hampshire. GUMICS was developed by Pekka Janhunnen et al. at the Finnish Meteorological Institute. This work was carried out using the SWMF and BATS-R-US tools developed at the University of Michigan's Center for Space Environment Modeling (CSEM). The modeling tools described in this publication are available online through the University of Michigan for download and are available for use at the Community Coordinated Modeling Center (CCMC).

References

Bonde, R. E. F., Lopez, R. E., & Wang, J. Y. (2018). The effect of IMF fluctuations on the subsolar magnetopause position: A study using a global MHD model. *Journal of Geophysical Research: Space Physics*, *123*(4), 2598–2604. https://doi.org/10.1002/2018JA025203

Borovsky, J. E. (2008). Flux tube texture of the solar wind: Strands of the magnetic carpet at 1 AU? *Journal of Geophysical Research*, *113*(A8), A08110. https://doi.org/10.1029/2007ja012684

Collado-Vega, Y. M., Dredger, P. M., Lopez, R. E., Khurana, S., Rastaetter, L., Sibeck, D., & Anastopulos, M. (2023). Magnetopause stand-off position changes and geosynchronous orbit crossings: Models and observations. *Space Weather*, *21*, e2022SW003266. https://doi.org/10.1029/2022SW003212

Cramer, W., Raeder, J., Toffoletto, F., Gilson, M., & Hu, B. (2017). Plasma sheet injections into the inner magnetosphere: Two-way coupled openGGCM-RCM model results: OpenGGCM-RCM plasma sheet injections. *Journal of Geophysical Research: Space Physics*, *122*(5), 5077–5091. https://doi.org/10.1002/2017JA024104

Dmitriev, A., Suvorova, A., & Chao, J. (2011). A predictive model of geosynchronous magnetopause crossings. *Journal of Geophysical Research*, *116*(A5), A05208. https://doi.org/10.1029/2010JA016208

Janhunen, P., Palmroth, M., Laitinen, T., Honkonen, I., Juusola, L., Facsko, G., & Pulkkinen, T. (2012). The GUMICS-4 global MHD magnetosphere-ionosphere coupling simulation. *Journal of Atmospheric and Solar-Terrestrial Physics*, *80*, 48–59. https://doi.org/10.1016/j.jastp.2012.03.006

Lopez, R. E., Hernandez, S., Wiltberger, M., Huang, C. L., Kepko, E. L., Spence, H., et al. (2007). Predicting magnetopause crossings at geosynchronous orbit during the Halloween storms. *Space Weather*, *5*(1), 01005. https://doi.org/10.1029/2006SW000222

Lyon, J., Fedder, J., & Mobarry, C. (2004). The Lyon-Fedder-Mobarry (LFM) global MHD magnetosphere simulation code. *Journal of Atmospheric and Solar-Terrestrial Physics*, *66*(15–16), 1333–1350. https://doi.org/10.1016/j.jastp.2004.03.020

Maltsev, Y. P., Arykov, A. A., Belova, E. G., Gvozdevsky, B. B., & Safargaleev, V. V. (1996). Magnetic flux redistribution in the storm time magnetosphere. *Journal of Geophysical Research*, *101*(A4), 7697–7704. https://doi.org/10.1029/95JA03709

Maltsev, Y. P., & Lyatsky, W. B. (1975). Field-aligned currents and erosion of the dayside magnetosphere. *Planetary and Space Science*, *23*(9), 1257–1260. https://doi.org/10.1016/0032-0633(75)90149-x

Martyn, D. F. (1951). The theory of magnetic storms and auroras. *Nature*, *167*(4259), 92–94. https://doi.org/10.1038/167984b0

Merkin, V. G., Anderson, B. J., Lyon, J. G., Korth, H., Wiltberger, M., & Motoba, T. (2013). Global evolution of Birkeland currents on 10 min timescales: MHD simulations and observations. *Journal of Geophysical Research: Space Physics*, *118*(8), 4977–4997. https://doi.org/10.1002/jgra.50466

Merkin, V. G., & Lyon, J. G. (2010). Effects of the low-latitude ionospheric boundary condition on the global magnetosphere. *Journal of Geophysical Research*, *115*(A10), A10202. https://doi.org/10.1029/2010JA015461

Mukhopadhyay, A., Welling, D. T., Liemohn, M. W., Ridley, A. J., Chakraborty, S., & Anderson, B. J. (2020). Conductance model for extreme events: Impact of auroral conductance on space weather forecasts. *Space Weather*, *18*(11), e2020SW002551. https://doi.org/10.1029/2020SW002551

NASA CDAWeb Development Team. (2019). *CDAWeb: Coordinated data analysis web*. Astrophysics Source Code Library. record ascl:1904.006.

Pembroke, A., Toffoletto, F., Sazykin, S., Wiltberger, M., Lyon, J., Merkin, V., & Schmitt, P. (2012). Initial results from a dynamic coupled magnetosphere-ionosphere-ring current model. *Journal of Geophysical Research*, *117*(A2), A02211. https://doi.org/10.1029/2011JA016979

Powell, K. G., Roe, P. L., Linde, T. J., Gombosi, T. I., & De Zeeuw, D. L. (1999). A solution-adaptive upwind scheme for ideal magnetohydrodynamics. *Journal of Computational Physics*, *154*(2), 284–309. https://doi.org/10.1006/jcph.1999.6299

Raeder, J., Larson, D., Li, W., Kepko, E. L., & Fuller-Rowell, T. (2008). Openggcm simulations for the themis mission. *Space Science Reviews*, *141*(1), 535–555. https://doi.org/10.1007/s11214-008-9421-5

Raeder, J., McPherron, R., Frank, L., Kokubun, S., Lu, G., Mukai, T., et al. (2001). Global simulation of the geospace environment modeling substorm challenge event. *Journal of Geophysical Research*, *106*(A1), 381–395. https://doi.org/10.1029/2000ja000605

Redmon, R. J., Loto'aniu, P. T. M., & Singer, H. J. (2017). Magnetometer high-resolution level 2 data for GOES-I through GOES-P, provided in four coordinate frames [Dataset]. NOAA National Centers for Environmental Information. https://doi.org/10.7289/V5JM27WK

Ridley, A. J., De Zeeuw, D. L., Gombosi, T. I., & Powell, K. G. (2001). Using steady state MHD results to predict the global state of the magnetosphere-ionosphere system. *Journal of Geophysical Research*, *106*(A12), 30067–30076. https://doi.org/10.1029/2000JA002233

Ridley, A. J., Gombosi, T. I., & DeZeeuw, D. L. (2004). Ionospheric control of the magnetosphere: Conductance. *Annales Geophysicae*, *22*(2), 567–584. https://doi.org/10.5194/angeo-22-567-2004

Ridley, A. J., & Liemohn, M. W. (2002). A model-derived storm time asymmetric ring current driven electric field description. *Journal of Geophysical Research*, *107*(A8), SMP2-1–SMP2-12. https://doi.org/10.1029/2001JA000051

Sibeck, D. G. (1995). Demarcating the magnetopause boundary. *Reviews of Geophysics*, *33*(S1), 651–655. https://doi.org/10.1029/95rg00285

Sibeck, D. G., Lopez, R. E., & Roelof, E. C. (1991). Solar wind control of the magnetopause shape, location, and motion. *Journal of Geophysical Research*, *96*(A4), 5489–5495. https://doi.org/10.1029/90JA02464

Toffoletto, F., Sazykin, S., Spiro, R., & Wolf, R. (2003). Inner magnetospheric modeling with the rice convection model. *Space Science Reviews*, *107*(1/2), 175–196. https://doi.org/10.1023/A:1025532008047

Tóth, G., Sokolov, I. V., Gombosi, T. I., Chesney, D. R., Clauer, C. R., De Zeeuw, D. L., et al. (2005). Space weather modeling framework: A new tool for the space science community. *Journal of Geophysical Research*, *110*(A12), A12226. https://doi.org/10.1029/2005JA011126

Tóth, G., van der Holst, B., Sokolov, I. V., De Zeeuw, D. L., Gombosi, T. I., Fang, F., et al. (2012). Adaptive numerical algorithms in space weather modeling. *Journal of Computational Physics*, *231*(3), 870–903. https://doi.org/10.1016/j.jcp.2011.02.006

Wiltberger, M., Lopez, R., & Lyon, J. (2003). Magnetopause erosion: A global view from MHD simulation. *Journal of Geophysical Research*, *108*(A6), 1235. https://doi.org/10.1029/2002ja009564

Wolf, R. A., Harel, M., Spiro, R. W., Voigt, G.-H., Reiff, P. H., & Chen, C.-K. (1982). Computer simulation of inner magnetospheric dynamics for the magnetic storm of July 29, 1977. *Journal of Geophysical Research*, *87*(A8), 5949–5962. https://doi.org/10.1029/JA087iA08p05949

Zeeuw, D., Sazykin, S., Wolf, R., Gombosi, T., Ridley, A., & Toth, G. (2004). Coupling of a global MHD code and an inner magnetosphere model: Initial results. *Journal of Geophysical Research*, *109*, A12219. https://doi.org/10.1029/2003JA010366